J2.3 IMPACT OF A WIND-MASS ERROR ANALYSIS SCHEME ON FORECAST SKILL

Lars Peter Riishojgaard, Runhua Yang*, Jing Guo
Global Modeling and Assimilation Office,
NASA-GSFC, Greenbelt, MD

1. INTRODUCTION

The way in which the statistical relationship between wind and height errors is modeled is an important attribute of any atmospheric data analysis system. Often it is assumed that this relationship – at least in the extratropics – closely mimics the near-geostrophic relationship between the wind and height fields themselves, and therefore also that the wind error is dominated by errors in the rotational wind (e.g., Hollingsworth and Lönnberg 1986; Lönnberg and Hollingsworth 1986). However, in practice it is difficult to provide a robust quantitative partioning of the wind error into geostrophic and ageostrophic compononents and rotational and irrotational components. A number of different methods are widely used to provide parameter estimates for background error covariances used in meteorological analysis schemes. One of these, the so-called NMC method (Parrish and Derber, 1992), provides global multivariate correlations valid for the full horizontal and vertical extent of the model domain, and has been adopted by several weather forecast operational centers. The basic assumption behind the method is that differences between forecasts at different ranges valid at the same time can be used as proxies for actual forecast errors. Such lagged-forecast differences are easy to obtain and it is easy to generate whichever statistics are required from them. On the other hand, the basic assumption may seem difficult to justify, and error statistics obtained by this method typically need to be scaled using some form of independent information in order to represent the 6-hour forecast errors required for data assimilation applications. In practice, error covariance statistics are most often built using a variety of different methods applied at the discretion of the experimenter. The ultimate test of the error statistics lies in the performance obtained with them rather than in any intrinsic superiority of the method by which they were obtained.

In this study we propose an improvement to the wind-mass balance scheme used in the operational version of Physical-Space Statistical Analysis System (PSAS) of the Global Modeling and Assimilation Office (GMAO). There are two components to the changes: one is that the coupling between the wind and mass errors is weakened in the extratropics; the other is that the error in the divergent wind component is increased. These changes to the wind-mass error statistics were based on NMC method statistics as well as anecdotal evidence of spurious mass analysis increments due to wind observations using the old wind-mass balance. Two-month assimilation runs with 5-day forecast runs launched every other day were performed with both the old wind-mass balance ('control') and the revised scheme ('perturbation'). In order to assess the impact of the new scheme, both forecast output and analysis fields were compared between the control and perturbation experiments. The metrics for assessment include standard forecast skill scores, innovation ("Observation minus Forecast") statistics, as well as subjective evaluation of certain features in the fields and in the general circulation as depicted in the two experiments. For the latter part of the assessment, global analysis fields provided by the National Centers for Environment Prediction (NCEP) are used as a reference.

2. METHOD AND EXPERIMENTAL DESIGN

2.1 Height-wind Forecast Error Analysis Scheme

In the PSAS algorithm, a multivariate wind-height error covariance is applied to wind and height analysis. The algorithm can – at least in principle – accommodate a flexible three-dimensional error specification since the analysis equation is solved in observation space. The wind error is given as the sum of two components: one is coupled to the geopotential height error through a basic mass-wind balance relation (geostrophy), while the other is uncoupled from

*Additional affiliation: Science Systems and Applications Inc., Lanham, MD

errors in the mass field (Guo et al. 1998). The mass-coupled wind errors (u_c, v_c) are modeled in terms of the height error h by assuming the following linear relationship:

$$\begin{bmatrix} u_c \\ v_c \end{bmatrix} \equiv \frac{g}{2\Omega a} \begin{bmatrix} \alpha_{um} & \alpha_{ul} \\ \alpha_{vm} & \alpha_{vl} \end{bmatrix} \begin{bmatrix} h_m \\ h_l \end{bmatrix}. \quad (1)$$

The height-decoupled wind errors (u_d, v_d) are specified as:

$$\begin{bmatrix} u_d \\ v_d \end{bmatrix} \equiv \frac{g}{2\Omega a} \begin{bmatrix} -\psi_m + \chi_l \\ \psi_l + \chi_m \end{bmatrix}. \quad (2)$$

Here, α_{um}, α_{ul}, α_{vm} and α_{vl} are coefficients coupling the height error gradient in the meridional (m) or longitudinal (l) direction to the error in the u and v components, respectively. Note that these coupling coefficients are assumed to be functions of latitude and pressure level. The acceleration due to gravity is denoted by g, Ω is the angular velocity of the rotation of the Earth, and a is the radius of the Earth. The stream function and velocity–potential of the mass-decoupled wind errors are denoted by ψ and χ, respectively, and $h_m \equiv \partial_m h$; $h_l \equiv \partial_l h$; $\psi_m \equiv \partial_m \psi$; $\psi_l \equiv \partial_l \psi$; $\chi_m \equiv \partial_m \chi$; and $\chi_l \equiv \partial_l \chi$. The symbols ∂_m and ∂_l denote differentiation operators, defined as

$$\partial_m(\cdot) \equiv \frac{\partial(\cdot)}{\partial \varphi}, \quad (3)$$

$$\partial_l(\cdot) \equiv \frac{\partial(\cdot)}{\cos\varphi \partial \lambda}. \quad (4)$$

The NMC Method was applied to output from a one-month assimilation/forecast run for January 2002 with the GMAO PSAS system. Difference fields between 24- and 48-hour forecasts valid for the same verification time were considered to be forecast errors. The first step was to derive the four coupling coefficients from height difference gradients. Since the coupling coefficients are functions of latitude, this estimation was performed in 5^0-latitude bins. As a next step, the coupled wind was computed, and the decoupled wind was then calculated as the difference between the total wind error and the coupled wind error. The decoupled wind is further partitioned into rotational and divergent components.

2.2 Comparison of Wind Error Components

Figure 1 shows the coupling ratio defined as the ratio of mass-coupled wind error variance to total wind error variance. The top panel shows this quantity as derived using the NMC method. The

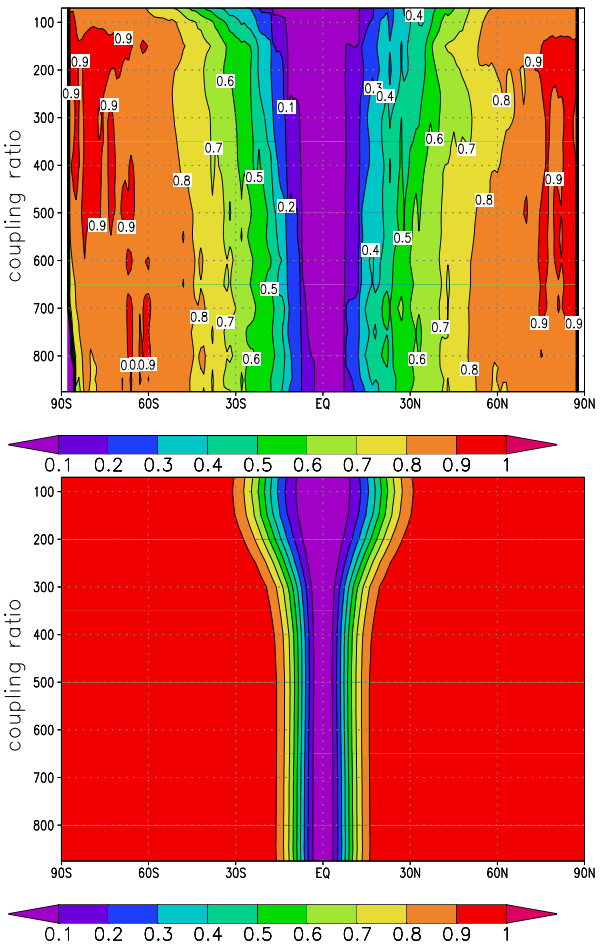

Figure 1: The ratio of coupled wind error variance to total wind error variance. Top: derived from "NMC" method; bottom: from the control experiment.

ratio is zero over the equator and increases with latitude. In the mid-latitudes, the coupling ratio lies in the 0.6-0.8 range, decreasing slightly in the upper troposphere. The bottom panel shows the coupling ratio as defined by the wind-mass balance scheme used in the control run. There are two striking features in this figure: the ratio increases sharply with latitude, reaching a value of 0.7 already at about 15^o of latitude, and the values remain above 0.9 in the mid-latitudes throughout the vertical extent of the domain.

Figure 2 shows the time-average of the zonal magnitude of the divergence derived from the total wind increment for January 2002, based on 15 samples. The top panel shows the NCEP analyses

and the bottom shows the control. The amount of divergence increment in the control is consistently significantly smaller than that of NCEP, and there is no indication in the control of a maximum near the jet stream region of the winter mid-latitude tropopause. The magnitude of the corresponding vorticity fields derived from the wind increments is very similar between the control and NCEP.

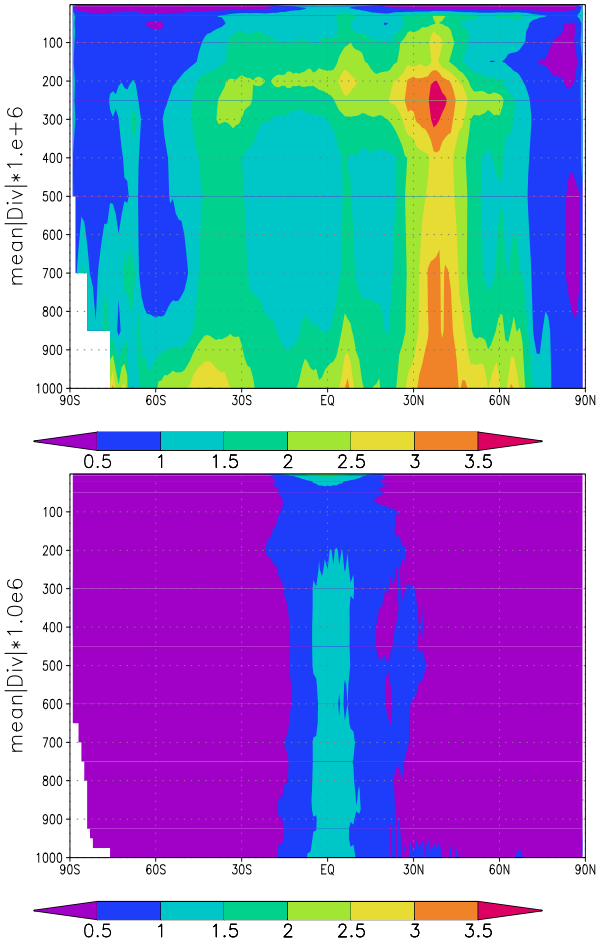

Figure 2: Zonally time mean of divergent magnitude derived from the wind analysis increment for Jan. 2002 (15 samples). top: NCEP analysis output; bottom: the control experiment

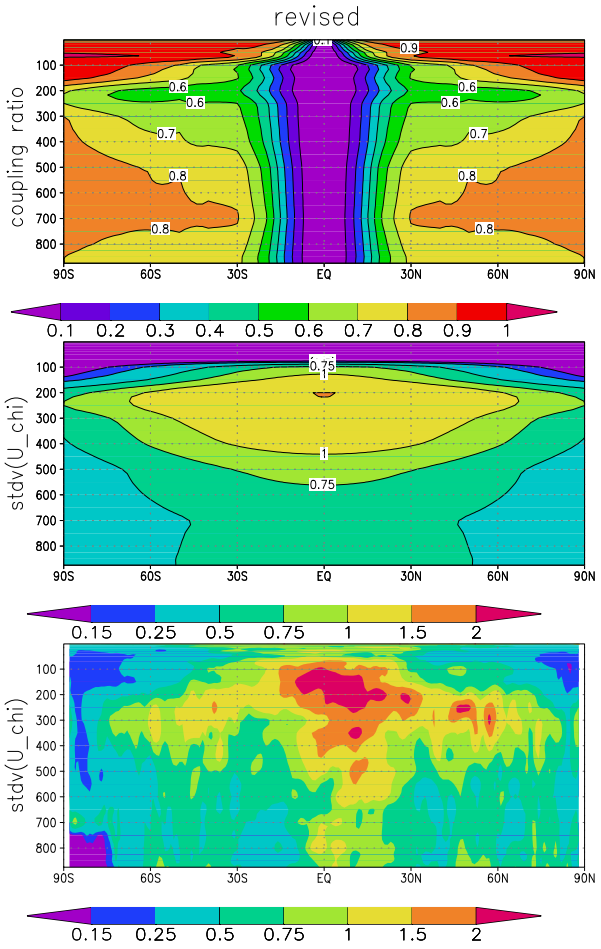

Figure 3: The coupling ratio (top) and standard deviation of divergent wind error (middle) used in perturbation experiment; bottom: the standard deviation of divergent wind error (decoupled) derived from NMC method.

Based on this comparison and a study of observational data (da Silva, personal communication), a decision was made to modify the wind-mass scheme in two respects: reducing the coupling in the extratropics, and increasing the divergent component

of the wind error based on the NMC results. The forecast height errors were changed accordingly. The revised coupling ratio and wind error components are shown in Figure 3.

2.3 Experimental Design

Assimilation experiments for the months of January and February 2002 were carried out using the revised mass-wind balance scheme and the control. In each experiment, a five-day forecast was launched from the 00Z analysis on the even dates. All the commonly used observation types were included in the assimilations: conventional surface data, radiosondes, aircraft data, satellite mass, wind, and humidity observations, etc.

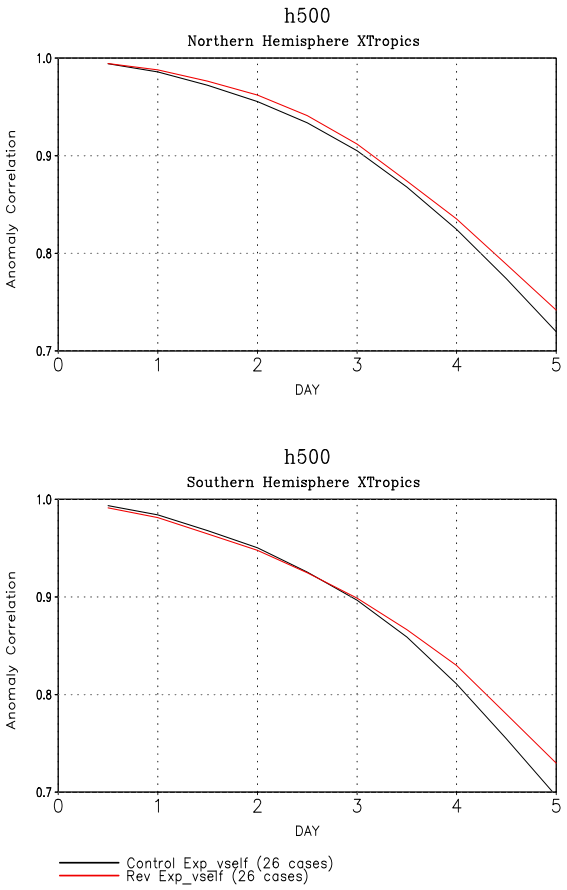

Figure 4: Anomaly correlation over the Northern Hemisphere and the Southern Hemisphere at 500 hPa with 26 cases. Red curves for the new experiment, and black ones for the control.

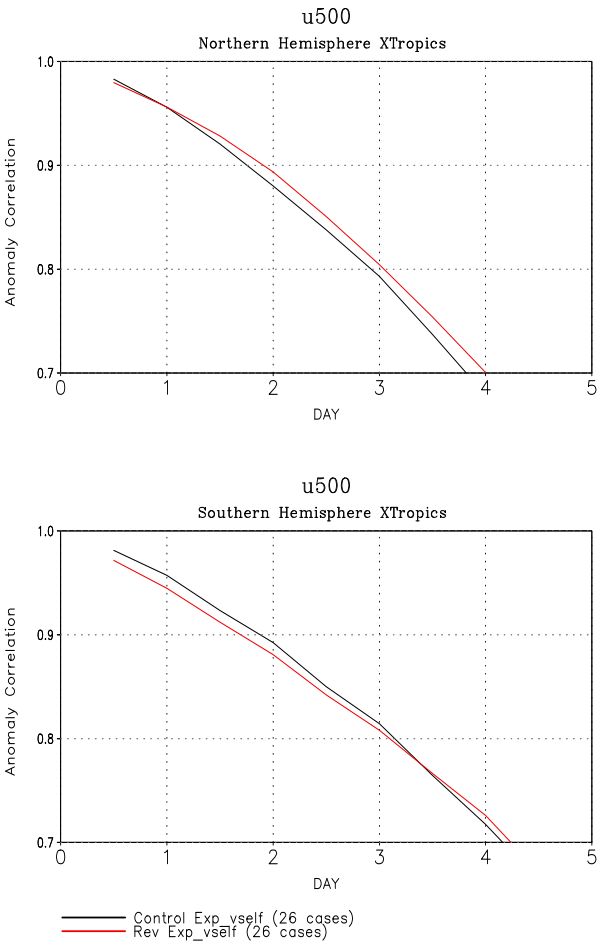

Figure 5: Anomaly correlation over the tropical region, the Northern Hemisphere and the Southern Hemisphere at 500 hPa with 26 cases.

3. EXPERIMENTAL RESULTS

For this study the primary performance metric for the scheme is its ability to produce good five-day forecasts. Figure 4 shows the anomaly correlation for forecasts from each experiment verified against their own analyses in the extratropical regions (30^0 -60^0) of both hemisphere at 500 hPa. The correlation of the perturbation experiment (red line) is consistently higher than that of the control after day two. Similar improvement is depicted at 300hPa and 200hPa.

Similarly, Fig.5 shows anomaly correlations for the zonal wind component at 500 hPa. The correlation is improved consistently in the northern hemisphere extratropics. Significant improvement occurs over the

tropics (30^0S-30^0N). However, the correlations in the southern hemisphere are slightly degraded. Similar results hold for 200 hPa and for the meridional component of the wind (not shown). The standard deviations of wind error of the new experiment are consistently lower than that of the control experiment. Anomaly correlations based on verification against NCEP analyses were also calculated for both the control and perturbation experiments. Again it was found that the anomaly correlations of the perturbation experiment tended to be higher than in the control, in agreement with the self-verification results.

Figure 6 shows the standard deviation of the wind innovations (observation minus forecast) for the month of February 2002. The observations used here are radiosondes. In general, the innovations are smaller in the pertubation experiment than in the control for all regions of the globe. This indicates that the new wind-mass scheme leads to a short-range forecast that is in better agreement with the observations. For the geopotential heights the difference between the standard deviation of the innovations from the control and perturbation are very small.

In order to examine the day to day variability of the forecast skill, time series for the day five anomaly correlations were plotted. Figure 7 shows an example of this, namely the 500 hPa height anomaly correlations over the Northern Hemisphere (top panel) and the Southern Hemisphere (bottom). It is clear that the perturbation experiment represents an improvement in most cases, although there are no striking inconsistencies between the skill of the two experiments.

We also examined certain characteristics of the general circulation as depicted by the two sets of analyses, using NCEP analysis fields as a reference. Figure 8 shows the zonal mean magnitude of the divergence (top panel) and vorticity (middle) derived from the wind analysis increment of the perturbation experiment. The bottom panel shows the magnitude of the vorticity magnitude in the NCEP analyses increment. Comparing with the NCEP divergence increments discussed earlier (top panel of Fig.2), we see that the perturbation experiment does produce a tropopause maximum, albeit of significantly smaller magnitude. As mentioned in Section 2, the vorticity of the analysis increment between the control and the NCEP is similar. In the perturbation experiment this similarity is retained (middle and bottom panels). //

4. DISCUSSION

This study shows the impact of a revised wind-mass scheme on both analysis and forecast integrations. The scheme is derived using the NMC method in conjunction with empirical considerations. The degree of assumed geostrophy in the error and the variation thereof with latitude and altitude is the primary factor controlling the dynamical impact of wind and mass observations. The revised scheme reduces the height and wind forecast error over the Northern Hemisphere, but not over the Southern Hemisphere. Increasing the divergent component of the wind error seems to improve the overall circulation patterns of the analyses. However, some other important parameters are not discussed here, such as correlation functions and the possibility of including a flow-dependence in the forecast error statistics. We plan to continue the study by combing NMC method and observational method to obtain a consistent forecast error estimate, and to fully test and examine their impact.

References

Guo, J., J. W. Larson, G. Gaspari, A. da Silvar, and P. M. Lyster, 1998: Documentation of the physical-space statistical analysis system (PSAS). Part II: The factored-operator formulation of error covariances. *DAO Office note*, **1998-04**.

Hollingsworth, A., and P. Lönnberg, 1986: The statistical structure of short-range forecast errors as determined from radiosonde data. Part I: The wind field. *Tellus*, **38A**, 111-136.

Lönnberg, P., and A. Hollingsworth, 1986: The statistical structure of short-range forecast errors as determined from radiosonde data. Part II: The covariance of height and wind errors. *Tellus*, **38A**, 137-161.

Parrish, D. F., and J. C. Derber, 1992: The national meteorological center's spectral statistical-interpolation analysis system. *Mon. Wea. Rev.*, **120**, 1747-1763.

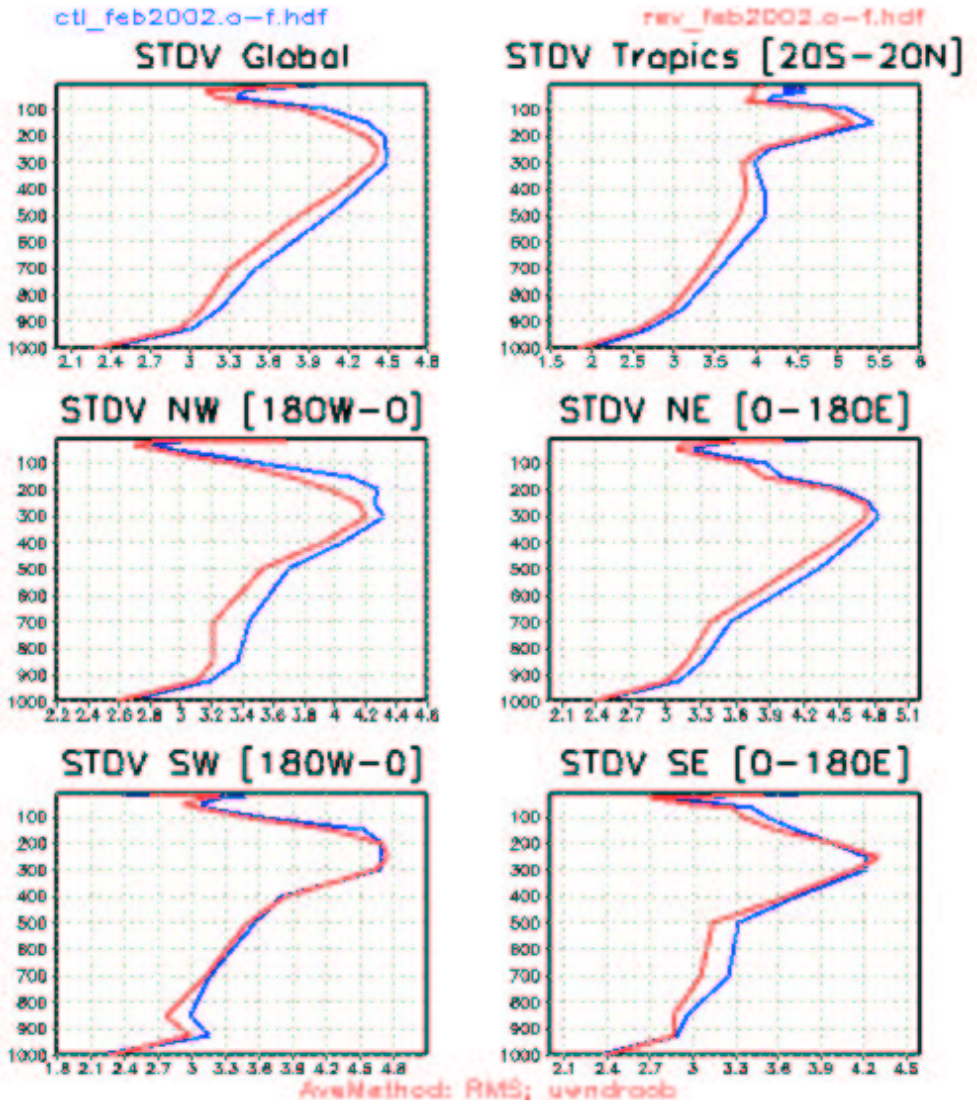

Figure 6: Standard deviation of the wind error derived from one month innovation for February 2002. The observation data are from rawinsondes. The blue lines for the control, and the red for the new experiment.

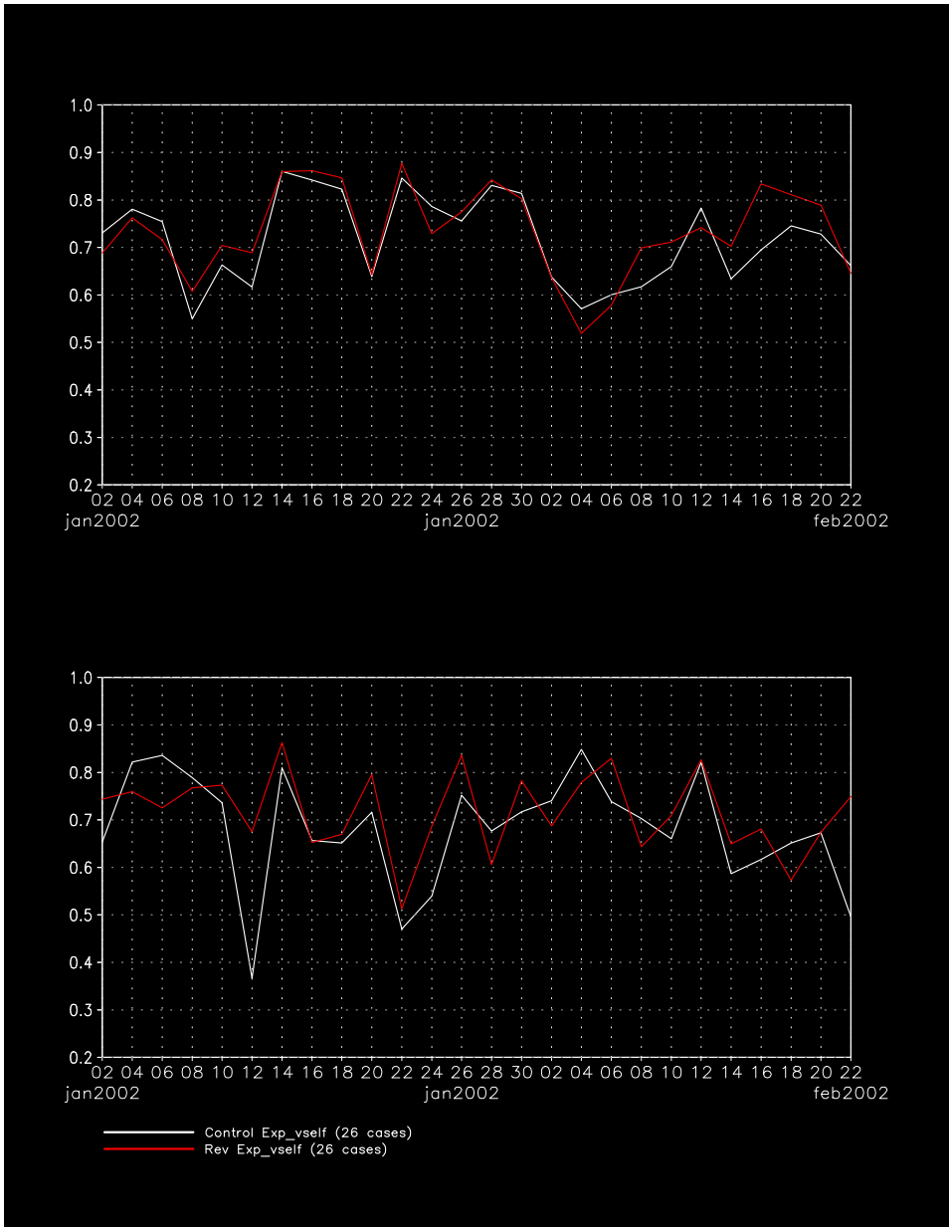

Figure 7: Time series of the anomaly correlation between day five forecast and its own assimilation for 500hPa height during the period of January and February 2002 for the Northern Hemisphere (top) and the Southern Hemisphere (bottom). Red line: perturbation experiment; white line: control experiment.

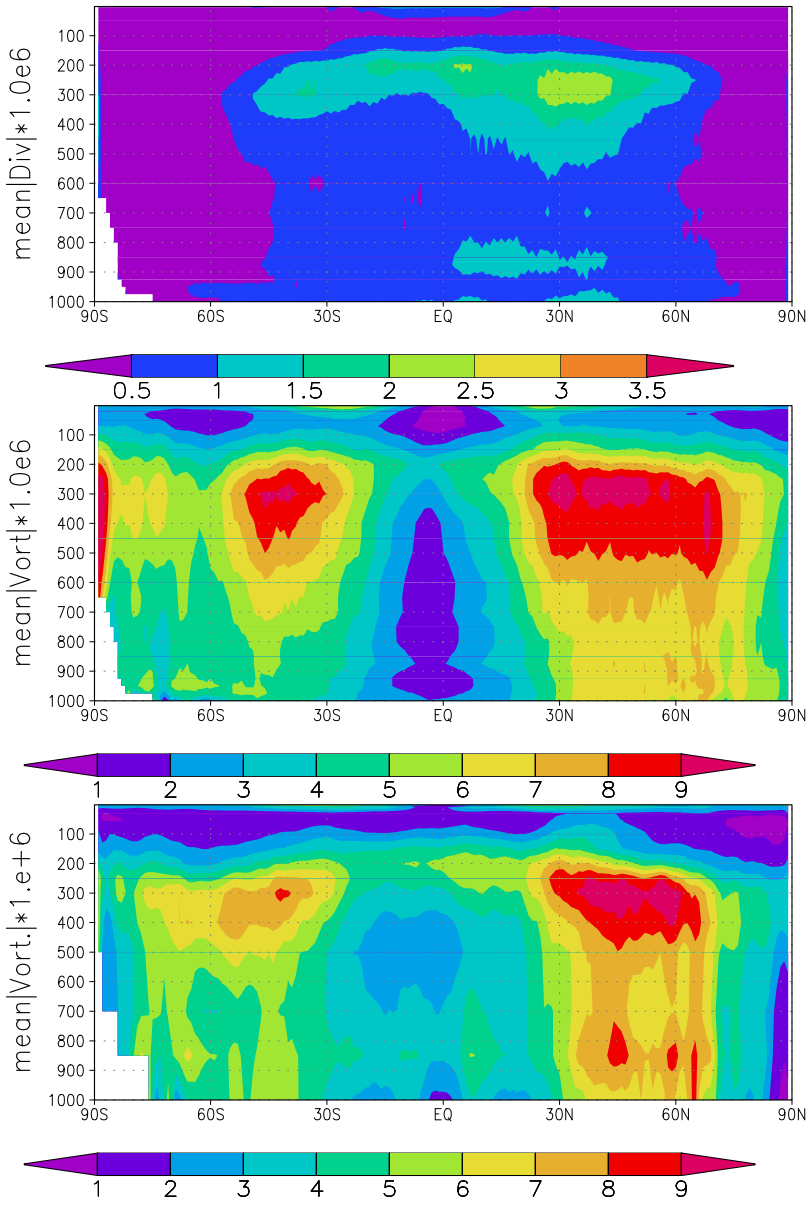

Figure 8: Zonally mean divergence magnitude (top panel) and vorticity (middle) derived from the analysis increment of the perturbation experiment. The bottom panel shows the vorticity magnitude derived from NCEP analysis increment. Results are derived from 15 samples.